**Supplementary Information**

**Surface characterization**

*XPS measurements*.

XPS measurements of gold surface after MUA and MUA/$(CH_2)_6$ OH immobilization and after nisin Z binding are illustrated in Figure S1 and summarized in Table S1. The XPS spectra of unmodified gold surfaces show C1s and O1s peaks, as expected when Au surface are not prepared in ultra-high vacuum conditions (13). They are mainly due to hydrocarbon impurities (C1s peak) and to -OH from water molecules (O1s peak). Comparison of the XPS data for the gold surfaces before and after MUA functionalization, revealed the appearance of a sulfur peak and the decrease of Au4f intensity both on Au-MUA and Au-MUA25 surfaces (Table S1), confirming immobilization of thiols on the gold surfaces (13,35,S1). The attenuation of the Au4f peak by the adlayer was more important for Au-MUA corresponding to a higher thickness of MUA layer compared to MUA25 (11 carbons for MUA chain vs 6 carbons for mercaptohexanol). The high resolution analysis of the S2p peaks (Table S2, Figure S1) reveals the presence of two sulfur components, one at 162.1 eV ($S2p_{3/2}$) and 163.4 eV ($S2p_{1/2}$) attributed to sulfur atoms bound to the gold surface (in red on Figure S1) and the second one at 163.7 eV ($S2p_{3/2}$) and 164.9 eV ($S2p_{1/2}$) corresponding to free thiol functions (in blue on Figure S1) (S2). The free thiols content was larger for Au-MUA (45%) compared to Au-MUA 25 (30%). The presence of free sulfur is probably due to the formation of a partial bilayer through hydrogen bonds between the carboxylic terminal groups of thiols bonded to the surface and free thiols from the solution (in this case, the S atom outwards from the surface). This was further confirmed by IR spectra analyses (see FTIR-ATR section). The high resolution XPS spectra of the C1s region for Au-MUA and Au-MUA25 substrates (Figure S1, Table S2), were best fitted with four components corresponding to C-C/C-H bonds at 285 eV, carbon in α position of heteroatom (S and O atoms) at 286.2 eV, carboxylate functions at 288 eV and carboxylic acid functions at 289.5 eV (35,S2). Percentages of the four components were different between MUA and MUA-25 (Table S2). A lower C-S/C-O component at 286.5 eV and higher C-C/C-H and COOH contributions at 285eV and 289.5 eV, were observed for the MUA layer. These differences can be explained by the longer alkyl chain average length for MUA and the lower carboxyl group concentration for Au-MUA25.

The success of nisin Z grafting on the two types of surfaces was confirmed by (i) the significant decrease of Au4f peak intensity, (ii) the appearance of a nitrogen peak (N1s) centered at 400.2 (Table S1, Figure S1) assigned to the amide functions of the peptide (35) and (iii) an approximatively twice larger free sulfur peak after nisin Z immobilization (Figure S1) due to

the presence of sulfur atoms from thioether functions in the peptide (16,17). These effects were more pronounced for Au-MUA-Nis surface by comparison to Au-MUA25-Nis.

*Table S1: Surface atomic composition of gold and modified gold surfaces determined by XPS The proportion of component composition from peak areas were performed using the CasaXPS software system and applying a Gaussian/Lorentzian ratio (70/30).*

| **Surfaces** | **Atomic composition (%)** | | | | |
|---|---|---|---|---|---|
| | Au 4f | C 1s | O 1s | S 2p | N 1s |
| **Gold** | 60.4 | 29.4 | 10.2 | - | - |
| **Au-MUA** | 46.8 | 38.1 | 13 | 2.1 | - |
| **Au-MUA25** | 57.8 | 27.3 | 12.3 | 2.6 | - |
| **Au-MUA-Nis** | 19.8 | 54.2 | 14.3 | 2.2 | 9.5 |
| **Au-MUA25-Nis** | 32.2 | 41.8 | 15.5 | 2.5 | 8 |

*Table S2: C1s and S2p chemical composition (%) of modified surfaces*

| | **Carbon components (%)** | | | | **Sulfur components (%)** | |
|---|---|---|---|---|---|---|
| **Surfaces** | C-C/C-H (285 eV) | C-S/C-O (286.5 eV) | $COO^-$/ N-C=O (288 eV) | COOH (289.5 eV) | S-Au (162.1 eV) | Free S (163.7 eV) |
| **Au-MUA** | 72.7 | 13.4 | 6.1 | 7.8 | 55.2 | 44.8 |
| **Au-MUA25** | 64.7 | 22.8 | 6.4 | 6.1 | 69.6 | 30.4 |
| **AU-MUA-Nis** | 59.1 | 23.7 | 15.6 | 1.6 | 28 | 72 |
| **Au-MUA25-Nis** | 56.5 | 26.7 | 15.3 | 1.5 | 45 | 55 |

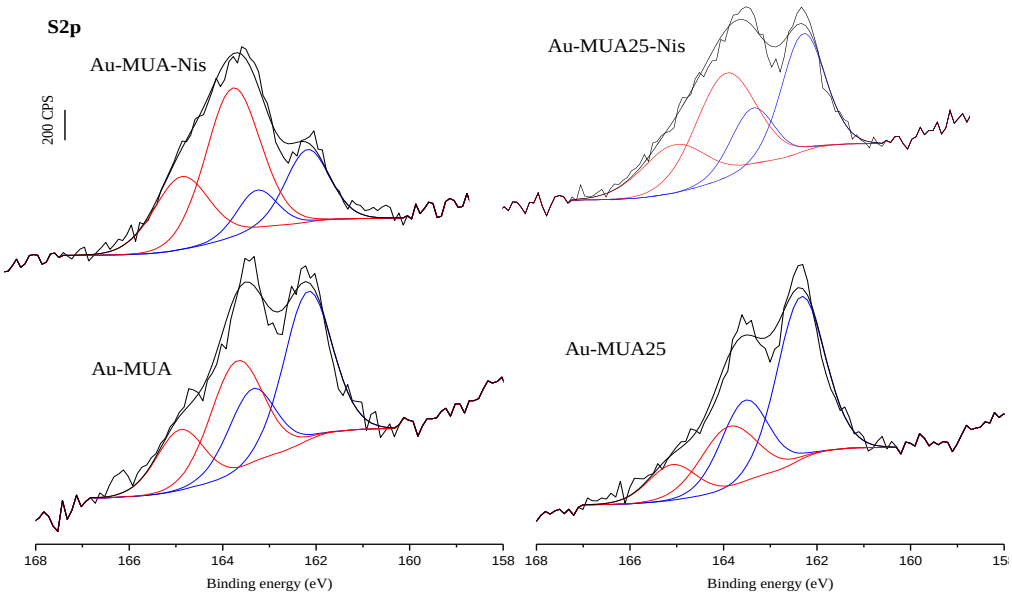
S2p
Au-MUA-Nis
200 CPS
Au-MUA25-Nis
Au-MUA
Au-MUA25
168
166
164
162
160
158
Binding energy (eV)

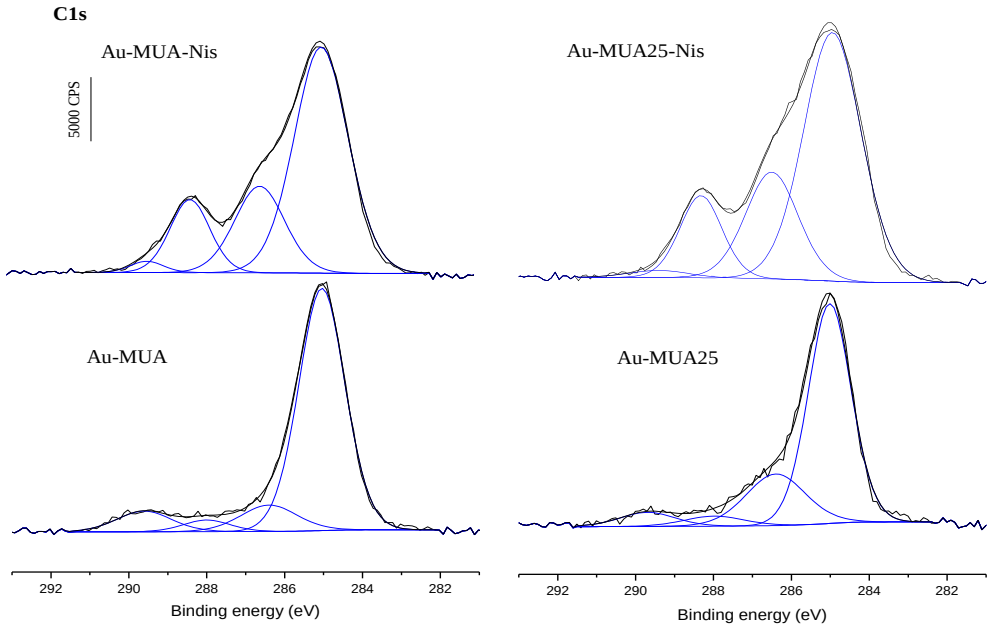
C1s
Au-MUA-Nis
5000 CPS
Au-MUA25-Nis
Au-MUA
Au-MUA25
292
290
288
286
284
282
Binding energy (eV)

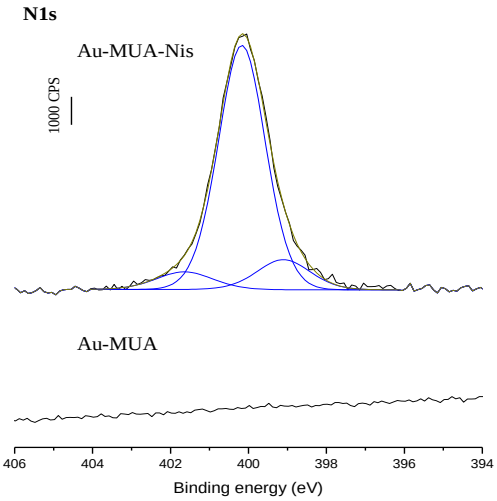
N1s
Au-MUA-Nis
1000 CPS
Au-MUA
406
404
402
400
398
396
394
Binding energy (eV)

*Figure S1: High resolution XPS spectra of S2p, C1s and N1s regions before and after nisin Z immobilization. The spectra were acquired with a Thermo Electron K-Alpha Spectrometer using a monochromatic Al-K-Alpha X-ray source (1486.6 eV) with a spot size of 400 µm, a pass energy of 50 eV and through a range of -10 to 1350 eV with pass energy of 200 eV. The binding energy was referenced by setting the maximum C 1s peak at 285.0 eV. The deconvolution of peaks from the spectra was performed using the CasaXPS software system and applying a Gaussian/Lorentzian ratio (70/30)*

*FTIR-ATR measurements*

*FTIR-ATR* measurements were obtained using a Brüker Vertex 70 FTIR spectrometer, equipped with an attenuated total reflection (ATR) accessory (PIKE MIRacle crystal plate diamond/ ZnSe) and a mercury cadmium telluride (MCT) detector cooled down by liquid nitrogen. 100 spectra were accumulated over the spectral region 3100 to 1400 $cm^{-1}$ with a spectral resolution of 4 $cm^{-1}$. The background was recorded (average of 100 scans) on the ATR unit without any substrate pressed against the crystal.

Infrared spectroscopy measurements further confirm the chemical composition of the surfaces at each step. The FTIR-ATR spectra for Au-MUA and Au-MUA25 showed similar peak positions in the C-H stretching region, corresponding to asymmetric (2928 $cm^{-1}$) and symmetric (2856 $cm^{-1}$) stretching modes of the $CH_2$ alkyl chains of MUA and 6-mercaptohexanol (Figure S2). The unexpected shoulder at 2960 $cm^{-1}$ corresponds to the asymmetric band of the methyl group. It was due to impurities related to MUA conditioning as revealed by the spectrum of a KBr pellet of MUA, where it is present (S1). The corresponding symmetric band of this methyl group is expected at ≈2880 $cm^{-1}$. It is not clearly visible, presumably because it is weaker than its asymmetric counterpart and is hidden in the wings of other bands. The frequency of the asymmetric methylene stretching is reported to be sensitive to conformational ordering: the more ordered the alkyl chain, the lower the frequency (2918 $cm^{-1}$ for a well-ordered alkyl chain) (S3). Therefore, the position of the asymmetric band of Au-MUA and Au-MUA25 before and after activation at 2928 $cm^{-1}$ suggests a certain disorder of the thiol layers. This was supported by the IR spectra measured in the frequency range 1800 $cm^{-1}$-1500 $cm^{-1}$. Figure S2). The two bands at 1742 $cm^{-1}$ and 1714 $cm^{-1}$ were attributed to the CO stretching mode of non-hydrogen-bonded and hydrogen-bonded carboxylic acid groups, respectively (,34, S4). The band at 1714 $cm^{-1}$ is consistent with the ability of carboxylic acids to undergo strong intermolecular hydrogen bounding interaction. This can occur from head to head MUA chain dimers forming a partial bilayer of MUA chains, as already suggested from XPS data. Nevertheless, dimerization of

carboxylic groups of neighboring MUA chains may also exist, which would imply disorder within the layer. Elsewhere, the large absorption signals in the range 1570-1540 $cm^{-1}$ and the band at 1463 $cm^{-1}$ are ascribed to the asymmetric and symmetric stretching modes of $COO^-$ respectively. It reveals that some deprotonated $COO^-$ groups are present. They are able to induce electrostatic repulsion and presumably a relative disorder of the surface layer (S5). SFG measurements further support this disorder of the Au-MUA and Au-MUA25 layers.

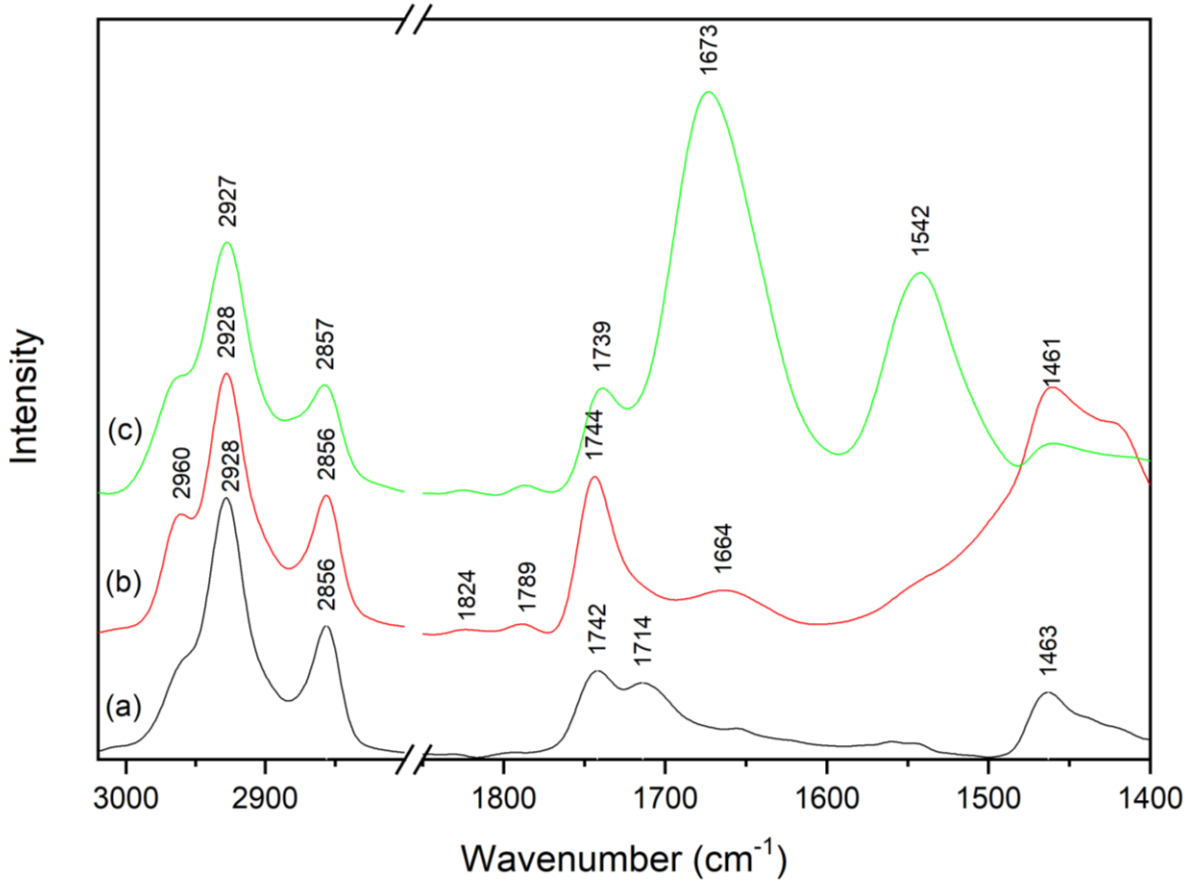


*Figure S2: FTTR-ATR spectra of the three consecutive steps leading to the nisin Z immobilization: (a) Au-MUA or Au-MUA25, (b) Au-MUA$_{act}$ or Au-MUA25$_{act}$ by NHS/EDC, (c) covalent binding of Nisin Z, Au-MUA-Nis or Au-MUA25-Nis.*

At the second step of surface preparation (termination by the succinimidyl ester), two more $CH_2$ groups (present in the succinimidyl cycle) are added on each MUA chain. However, their contribution to the $CH_2$ symmetric and asymmetric bands does not produce a quantitative change of relative intensities (Figure S2). By contrast, this attachment of the succinimidyl ester termination is evidenced by the triplet in the spectral range of the C=O stretching vibrations: (i) the persistence of the prominent peak at 1744 $cm^{-1}$ corresponding to the transformation of the acid terminal group into ester, (ii) the appearance of two weak bands at 1788 $cm^{-1}$ and 1820 $cm^{-1}$ [1], the signature of the ester groups of the imide ring (30,25,S5) (Figure S2). The disappearance

of the 1714 $cm^{-1}$ absorption band highlights that the activation leads to the disruption of intermolecular hydrogen bonds between carboxylic groups. Smaller broad bands observed in some experiments at 1656 $cm^{-1}$ and ~1550 $cm^{-1}$ (not visible in the spectra of Figure S2), evocative of amide I and amide II bands, respectively, can be ascribed to the limited formation of the stable N-acyl urea byproduct due to defects in the activated layer (30). Finally, the broad band extending between 1500 $cm^{-1}$ and 1400 $cm^{-1}$ corresponds to bending modes of the different CH bonds. It cannot be exploited because it shows no structure.

Although the nisin Z peptide has an appreciable number of CH, $CH_2$ and $CH_3$ groups in various positions with respect to amide groups, the CH stretching spectrum does not show any significant change (Figure S2). However, the nisin Z grafting is ascertained by the appearance of the two strong bands at 1673 $cm^{-1}$ and 1542 $cm^{-1}$ that can be ascribed to the amide I and amide II bands of the peptidic backbone. In addition, a band centered at ~1739 $cm^{-1}$ is still present. It may correspond to the free carboxylic group of the C-terminated part of Nisin and/or from remaining non-activated carboxylic groups.

*Water contact angle measurements*

Static water contact angle measurements of all samples were performed using a sessile drop technique with deionized water as a probe liquid. The instrument used was DSA 30S Krüss contact angle system goniometer. To check surface uniformity and reproducibility, six measurements were acquired on each of two different samples by depositing six droplets (2.5 µl milliQ water) at different points of the surface (11mm x 11mm).

Table 3 summarizes the changes in the water contact angles when moving from Au to functionalized substrates. In each case, the water contact angle values were constant over the entire sample surface demonstrating that the successive functionalization of the gold surfaces were homogeneous.

*Table S3: contact angle measurements*

| Surfaces | Water contact angle (±1.5°) |
|---|---|
| **Gold** | 86 |
| **Au-MUA** | 52 |
| **Au-MUA25** | 45 |
| **Au-MUA$_{act}$** | 61 |
| **Au-MUA25$_{act}$** | 51 |
| **Au-MUA-Nis** | 62 |
| **Au-MUA25-Nis** | 60 |

When the gold surface was modified by MUA, an increase of the surface hydrophilicity is observed due to the introduction of polar head groups (COOH) and the hydrophilicity of the mixed OH/COOH terminated surface (Au-MUA25) is higher than that of a COOH terminated surface (Au-MUA), which is consistent with the literature (12,S2). Upon EDC/NHS activation, the water contact angle increased by ~7-10°, indicating lower hydrophobicity of the surface due to the formation of the succinimide ester intermediate (13,S6). The nisin Z immobilization rendered the surfaces slightly less hydrophilic, as expected considering the amphiphilic nature of the peptide. No difference between Au-MUA and Au-MUA25 substrates was observed.

## REFERENCES


S1. de la Llave E, Herrera SE, Adam C, Méndez De Leo LP, Calvo EJ, Williams FJ. Molecular and electronic structure of osmium complexes confined to Au(111) surfaces using a self-assembled molecular bridge. J Chem Phys. 14 nov 2015;143(18):184703.

S2. Mendoza SM, Arfaoui I, Zanarini S, Paolucci F, Rudolf P. Improvements in the Characterization of the Crystalline Structure of Acid-Terminated Alkanethiol Self-Assembled Monolayers on Au(111). Langmuir. janv 2007;23(2):582-8.

S3. Nuzzo RG, Dubois LH, Allara DL. Fundamental studies of microscopic wetting on organic surfaces. 1. Formation and structural characterization of a self-consistent series of polyfunctional organic monolayers. J Am Chem Soc. janv 1990;112(2):558-69.

S4. Casford MTL, Ge A, Kett PJN, Ye S, Davies PB. The Structure of Lipid Bilayers Adsorbed on Activated Carboxy-Terminated Monolayers Investigated by Sum Frequency Generation Spectroscopy. J Phys Chem B. 27 mars 2014;118(12):3335-45.

S5. Methivier C, Beccard B, Pradier CM. In Situ Analysis of a Mercaptoundecanoic Acid Layer on Gold in Liquid Phase, by PM-IRAS. Evidence for Chemical Changes with the Solvent. :6.

S6. Afara N, Omanovic S, Asghari-Khiavi M. Functionalization of a gold surface with fibronectin (FN) covalently bound to mixed alkanethiol self-assembled monolayers (SAMs): The influence of SAM composition on its physicochemical properties and FN surface secondary structure. Thin Solid Films. nov 2012;522:381-9.